Article

Potential Sources of Particulate Iron in Surface and Deep Waters of the Terra Nova Bay (Ross Sea, Antarctica)

Paola Rivaro [1],*, Francisco Ardini [1], Davide Vivado [1], Roberto Cabella [2], Pasquale Castagno [3], Olga Mangoni [4] and Pierpaolo Falco [5]

[1] Department of Chemistry and Industrial Chemistry, University of Genova, 16146 Genova, Italy; ardini@chimica.unige.it (F.A.); davide.vivado@edu.unige.it (D.V.)
[2] Department of Earth, Environment and Life Sciences, University of Genova, 16132 Genova, Italy; roberto.cabella@unige.it
[3] Department of Sciences and Technology, Parthenope University of Naples, Centro Direzionale, Isola C4, 80143 Napoli, Italy; pasquale.castagno@gmail.com
[4] Departmentof Biology, University of Napoli Federico II, Complesso Universitario di Monte Sant'Angelo, 80134 Napoli, Italy; olga.mangoni@unina.it
[5] Department of Life and Environmental Sciences, University Politecnica delle Marche, 60131 Ancona, Italy; pierpaolo.falco@staff.unipvm.it
* Correspondence: paola.rivaro@unige.it; Tel.: +39-010-355-6172

check for updates

Abstract: The distribution of particulate Fe (pFe), suspended particulate matter (SPM), and other particulate trace metals were investigated in Terra Nova Bay as part of CDW Effects on glaciaL mElting and on Bulk of Fe in the Western Ross sea (CELEBeR) and Plankton biodiversity and functioning of the Ross Sea ecosystems in a changing Southern Ocean (P-ROSE) projects. Variable concentrations of SPM (0.09–97 mg L^{-1}), pFe (0.51–8.70 nM) and other trace metals were found in the Antarctic Surface waters (AASW) layer, where the addition of meltwater contributed to the pool with both lithogenic and biogenic forms. The deeper layer of the water column was occupied by High Salinity Shelf Water (HSSW) and Terra Nova Bay Ice Shelf Water (TISW) encompassing glacial water as confirmed by the lightest $\delta^{18}O$ measured values. The concentration of pFe in TISW (11.7 ± 9.2 nM) was higher than in HSSW samples (5.55 ± 4.43 nM), suggesting that the drainage of material released from glaciers surrounding the area is relevant in terms of pFe contribution. Particulate Fe/Al and Mn/Al ratios were substantially in excess compared with the mean crustal ratios. Microscopic analyses confirmed that more labile Fe oxyhydroxides and authigenic MnO_2 phases were present together with biogenic sinking material. Future expected increasing melt rates of these glaciers enlarge Fe input, thus having a greater role in supplying iron and counteracting the reductions in sea ice cover around Terra Nova Bay.

Keywords: iron; suspended particulate matter; antarctica; ross sea

1. Introduction

In recent years, iron has been recognized as a key element in ocean biogeochemical cycles, particularly in High Nutrient Low Chlorophyll areas. The abundance and availability of iron (Fe) in sea water is controlled by a complex set of processes including biological utilization and export, interactions with particulate matter and complexing organic molecules, and aeolian deposition of iron-rich dust [1]. Fe biogeochemistry in the Ross Sea has been investigated in some recent studies, with particular attention to dissolved Fe (dFe) [2,3]. Field observations and model simulations indicate

four potential sources of dFe in Ross Sea surface waters: Circumpolar Deep Water (CDW) originating from the shelf edge, sediments from shallow banks and near shore areas, melting sea ice around the perimeter of polynya and glacial meltwater from the Ross Ice Shelf (RIS) [3].

Fewer measurements of particulate Fe (pFe) than dFe have been reported in the Ross Sea. Despite this, the study of pFe is essential to better constrain the iron biogeochemical cycle [4–6]. Sea ice meltwater contributes to pFe in Ross Sea surface waters near the receding ice edge during the austral summer [7], while terrestrial material may influence metal distribution more than aeolian input in coastal areas [8]. De Jong et al., (2013) [4] acknowledged the importance of dust and sea ice melt as sources of iron in coastal surface waters, along with sediment re-suspension and the melting of icebergs and ice sheets.

Evidence of significant annual, interannual and decadal variability in Ross Sea water properties and sea ice characteristics emphasizes the region's sensitivity to changing oceanographic and atmospheric forcing [9]. In this context, one of the most important topics concerns the processes that supply biologically available Fe to the surface waters of the Ross Sea. For example, reductions in sea ice extent and convective mixing might be expected to decrease the supply of iron to surface waters during the phytoplankton growing season, although these impacts might be tempered by increased inputs of Fe rich glacial and sea ice meltwater [9].

On the west coast of the Ross Sea, several glaciers have high basal melt rates that could supply Fe to the surrounding waters [10]. Therefore, this flux could represent, on a local scale, a source of Fe that is likely to increase with ongoing climate change. Enhancement of this source of Fe may thus stimulate the carbon biological pump and may represent a mitigating feedback to the increase of atmospheric CO_2.

Terra Nova Bay (TNB) polynya is a coastal latent heat polynya located in the western Ross Sea. Fe biogeochemistry in surface waters of the TNB area has been investigated in some recent studies, with specific focus on dFe. Results suggested that this coastal area is dFe-repleted [11–14]. However, it is also important that pFe data are collected and evaluated to ensure that any such changes are reliably tracked and attributed, and that their impacts on the ecosystem are identified.

In this context, this paper reports the pFe data collected during the austral summer of 2017 with the aim to better understand iron biogeochemistry in the TNB area. The data will be discussed depending on water mass properties and considering possible sources of pFe. $H_2^{18}O/H_2^{16}O$ ratio ($\delta^{18}O$), particulate aluminum or other particulate trace metals data, and microscopic analysis of selected samples will be used to support the findings.

As an oceanographic study is multivariate by nature, a multivariate statistical technique (i.e., Principal Component Analysis) will be used to evaluate the relationships between variables and to highlight the differences between stations.

2. Materials and Methods

2.1. Study Area

TNB is a coastal latent heat polynya approximately 80 km × 30 km wide, located in the western sector of the Ross Sea at about 75 °S, 164 °E (Figure 1A), [15]. It is bounded by three steep glacier valleys, the Reeves Glacier and Priestley Glacier draining into the Nansen Ice Sheet (NIS) and the David Glacier terminating in the Drygalski Ice Tongue (DIT) [16]. The TNB polynya southern border is protected from sea ice lateral advection by the DIT, which extends in a south-eastern direction and the length of which determines the polynya size [17]. The TNB polynya plays an important role in shaping sea ice and ocean dynamics as well as in forming saline shelf water in the western Ross Sea. In fact, brine released during sea ice formation increases the salinity of subsurface waters, resulting in the formation of High Salinity Shelf Water (HSSW), the densest water mass of the Southern Ocean [15,18]. HSSW flows out from the Ross Sea at the Drygalski Trough mouth, where, due to tidal force, it descends along the slope and eventually mixes with the CDW to form Antarctic Bottom Water

(AABW) [19,20]. Recent observations show an increase in HSSW salinity with repercussions for AABW density [21,22]. During the summer (November to March), the TNB water column can be divided into two layers. The upper layer is occupied by the Antarctic Surface Water (AASW), which becomes fresher and warmer due to the sea ice melting and increasing solar radiation. The lower layer is mainly filled with HSSW, which is characterized by a potential temperature (θ) close to the surface freezing point ($T_f = -1.914$ °C for $p = 0$ dbar and S = 34.85) and salinity (S) higher than 34.62 [23]. However, at intermediate depths the lateral advection of the Terra Nova Bay Ice Shelf Water (TISW) coming from beneath the NIS can be detected. TISW has a temperature lower than the surface freezing point because of the interaction of salty HSSW with the base of the glacial ice [24]. Although TNB is smaller than the Ross Sea (RS) polynya, it is characterized by high rates of primary production during summer [25]. Phytoplankton blooms develop later in the year than in the RS polynya, and they are dominated by diatoms [26].
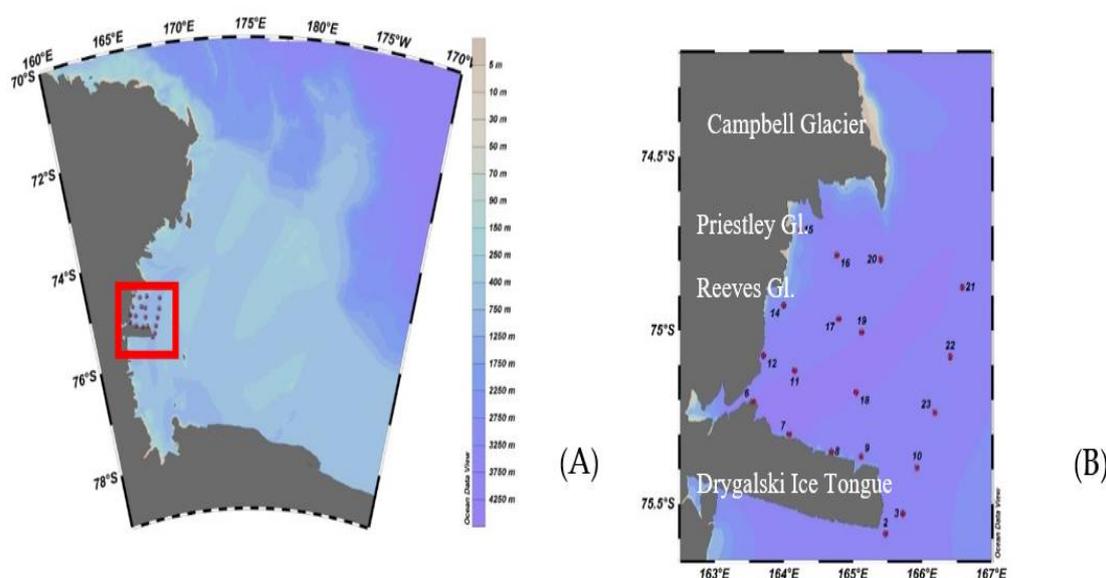

Figure 1. Map of the Ross Sea. (**A**) position of Terra Nova Bay in the Ross Sea (red square); (**B**) positions of sampled stations in the Terra Nova Bay area.

2.2. Sampling

Samples were collected onboard the R.V. Italica, as part of "CDW Effects on glaciaL mElting and on Bulk of Fe in the Western Ross sea"(CELEBeR) and "Plankton biodiversity and functioning of the Ross Sea ecosystems in a changing Southern Ocean" (P-ROSE) projects of the Italian National Program of Research in Antarctica (PNRA) from the 9th to the 15th of January 2017 (Figure 1B). Conductivity, temperature and depth were acquired using a CTD profiler, Sea Bird Electronics SBE 9/11plus. The CTD was equipped with two pairs of temperature-conductivity sensors, a SBE 23 O_2 sensor and a Chelsea Aquatrack III fluorometer for oxygen concentration and fluorescence data, respectively. CTD calibration was performed before and after the cruise. Data were acquired at the maximum frequency (24 Hz) with a descent speed of approximately 1 m s^{-1}. The data were corrected and processed according to recommended international procedures [27]. θ and S were computed using standard algorithms [28] and were processed and quality checked using CTD Sea Bird Electronics data processing software. Finally, resulting profiles were vertically averaged over 1 m depth bins. A SBE 32 plastic coated carousel sampler was used to collect water samples from twenty-four 12-L Niskin bottles. At selected depths (Table 1), seawater samples for iron analysis were collected by a 5-L teflon-lined GO-FLO bottle (General Oceanics Inc.), which was deployed on a Kevlar 6 mm diameter line and sealed using a polyvinyl chloride messenger. The GO-FLO bottle was covered with plastic bags after each station to minimize contamination. The effects of particle settling in the GO-FLO

bottle prior to filtration was minimized by gentle mixing of the sampling bottle prior to filtration [29]. Seawater was transferred in acid-cleaned 2-L low-density polyethylene bottles and filtered through acid-cleaned 0.45 μm pore-size polycarbonate (PC) membranes using a clean conditions filtration system, limiting filtration time to 1–2 h. This custom-built filtration apparatus was successfully tested for trace metal analysis of Antarctic water samples [12]. Therefore, in our study, suspended particulate matter (SPM) is operationally defined via the filtration of seawater as the material retained on 0.45 μm pore-size PC filters. Filters were gently rinsed with ultrapure water (Milli-Q from Millipore, El Paso, TX, USA) and placed in Petri dishes, sealed in double polyethylene bags and stored at −20 °C until analysis. In the laboratory, sample handling was performed in clean conditions under a Class−100 laminar flow hood. Before and after SPM collection, filters were weighed with a precision of ± 0.01 mg (Sartorius BP 210 D). Selected frozen filters were cut in four using a ceramic blade: one filter quarter was archived at −20 °C for electron microscopy analysis, while the remaining filters were dedicated to SPM total digestion.

Table 1. Sampling stations and depths for suspended particulate matter (SPM) and particulate metals analyses.

Station	Sampling Date	Latitude S (°)	Longitude E (°)	Bottom Depth (m)	Sampling Depth (m)
2	9 January 2017	−75.5858	165.4712	842	30–100–225–300
3	9 January 2017	−75.5273	165.7213	789	20–100–200–350
6	12 January 2017	−75.2055	163.5515	1108	20–100–240–320–440
7	12 January 2017	−75.2982	164.0772	1201	20–100–442
8	12 January 2017	−75.3495	164.6843	683	212–482
9	12 January 2017	−75.3630	165.1157	653	10–220–513
10	12 January 2017	−75.3947	165.9260	778	169–242–500
11	12 January 2017	−75.1160	164.1530	971	200–240–389
12	13 January 2017	−75.0720	163.7043	867	35–280–394
14	13January 2017	−74.9277	163.9963	342	20–205–320
15	13 January 2017	−74.7115	164.2308	498	40–200–390
16	13 January 2017	−74.7837	164.7640	771	20–300–379
17	14 January 2017	−74.9670	164.7920	919	20–240–300
19	14 January 2017	−75.0050	165.1255	925	20–191–400
20	14 January 2017	−74.7960	165.3995	662	20–288–330
21	14 January 2017	−74.8748	166.5780	886	30–300
22	15 January 2017	−75.0757	166.4043	854	15–300
23	15 January 2017	−75.2368	166.1813	852	15–252

2.3. Particulate Metals Analysis

SPM samples were solubilized with a mixture of nitric acid, hydrogen peroxide and hydrofluoric acid (2 mL of HNO_3, 0.5 mL of H_2O_2 and 0.2 mL of HF, Suprapur®-grade quality from Merck, Darmstadt, Germany) using the microwave digestion system MARS-5 (CEM, Matthews, NC, USA). Digested samples were then diluted to 10 mL with ultrapure water and analyzed by inductively coupled plasma atomic emission spectrometry (ICP-AES, Vista Pro, Varian Inc, Palo Alto, CA, USA). Table S1 reports the ICP-AES instrumental parameters. Accuracy and precision of the analytical procedure were verified using the certified reference material CRM-414 (marine plankton) provided by the Institute for Reference Materials and Measurements of the European Commission and by MURST-ISS-A1 (Antarctic bottom sediment) provided by the Italian National Institute of Health. Accordance with certified values (Table S2) demonstrates the absence of significant interferences and the completeness of the digestion. Filter digestion blanks amounted to 14.3 ± 1.7 ppb of Fe (n = 7), resulting in a detection limit (3σ of the blanks) of 0.1 nM. Together with pFe, particulates Al, Ba, Cd, Cu, Mn, Ni, Ti and Zn (hereafter pAl, pBa, pCd, pCu, pMn, pNi, pTi and pZn) were measured in order to support our assessment of pFe sources. Microscopic analyses of selected samples were performed by a field emission scanning electron microscope (FE-SEM), ZEISS SUPRA 40 VP coupled with an EDS (Energy Dispersive Spectroscopy) probe. For each sample, between 9 and 28 spectra were acquired.

2.4. Additional Parameters

Samples for the determination of $\delta^{18}O$ were collected from the Niskin bottles using a 15 mL conical polypropylene tube. $H_2^{18}O/H_2^{16}O$ ratio measurements were performed at the University of Tasmania (Australia). Subsamples (3.0 mL) were equilibrated with CO_2 at 25 °C with a VG Isoprep-18 equilibration bench. The oxygen isotope ratio of equilibrated CO_2 was measured on a VG Isogas SIRA mass spectrometer. The $\delta^{18}O$ values are expressed per mil (‰), relative to the Vienna Standard Mean Oceanic Water (V-SMOW) standard. The standard deviation (SD) of the $\delta^{18}O$ values for repeated measurements of laboratory reference water samples was less than 0.04‰. O_2 was measured on board using the Winkler method by automated micro-titrations [30] with a potentiometric detection of the end point using a Methohm 719 titroprocessor. The measurement precision was ±0.05 mg L^{-1}. Following the approach already used in our previous papers [13,31], we calculated the contribution of sea ice meltwater to surface waters in the upper surface layer (MW%) considering the difference between the salinity measured at the surface (S_{meas}) and the salinity measured in the same station at greater depth (S_{deep}), not influenced by sea-ice dilution and assuming an average sea-ice salinity of 6:

$$MW\% = \left(1 - \frac{S_{meas} - 6}{S_{deep} - 6}\right) \times 100 \tag{1}$$

In our study, S_{deep} depths were chosen based on their neutral density (γ^n) values [32], i.e., we chose samples collected below $\gamma^n = 28.00$ kg m^{-3}, which is the lower bound of the AASW [23].

2.5. Data Processing

Principal Component Analysis (PCA) was applied to the dataset in order to explore the correlations between particulate-bound metals, SPM and environmental parameters (sampling depth, salinity, temperature, $\delta^{18}O$, dissolved oxygen and fluorescence) in samples. First, data were normalized by log-transformation. Then, the data matrix, constituted by 53 rows (samples) and 20 columns (physical and chemical variables), was processed after autoscaling the data using the R-based software CAT [33].

3. Results

3.1. Water Masses

The θ–S diagram (Figure 2A) for all the stations sampled for trace metals shows the three main water masses in the TNB area. Following Orsi and Wiederwohl (2009) [23], the water masses were identified using θ, S and neutral density (γ^n). AASW is characterized by a $\gamma^n < 28.00$ kg m^{-3}, a θ between + 1.7 and −1.3 °C and an S lower than 34.4. The AASW occupies the upper layer of the water column with a thickness varying between 10 and 65 m, depending on the station considered. In the AASW, $\delta^{18}O$ ranged from −0.19‰ at station 8 to −0.44‰ at station 10 (Figure 2B). The contribution of sea ice meltwater to surface waters (MW%) is obviously greater at the surface (1.20 ± 0.59%) than at the subsurface depth sampled for particulate metals (0.89 ± 0.62%), but the difference is not statistically significant (Student's t-test, $p < 0.05$). A decrease in salinity greater than 1% occurred due to the contribution of sea ice meltwater at stations 9, 11, 12, 14, 18, 20, 21, 22 and 23, both at the surface and at the particulate metal sampling depth (Table 1 shows various sampling depths). Stations 2, 6, 7, 15, 16 and 19 did not show any recent decrease in salinity due to either glacial or sea ice melting, as suggested by the $\delta^{18}O$ isotopic ratio and MW% values lower than 1%. The deep layer of the water column was mainly occupied by HSSW and is characterized by θ below −1.85 °C and S greater than 34.62. HSSW has the highest γ^n value (>28.27 kg m^{-3}) due to its low temperature and high salinity (Figure 2A). TISW, identified by θ lower than −1.93 °C and S lower than that of the HSSW, was detected at some stations at intermediate depths (between 200 and 440 m). TISW was mainly found along the coast near the NIS, from the DIT to the Campbell Glacier Tongue (stations 6, 12, 14 and 15), but it was also observed further offshore in the northern part of the bay (stations 16, 17, 19 and 20). Figure 3

shows the lateral advection of the TISW from the coast toward the open ocean. No TISW was found offshore along the DIT (Stations 7, 8 and 9). TISW samples showed the lightest δ^{18}O values ($-0.6\permil$, Figure 2B).
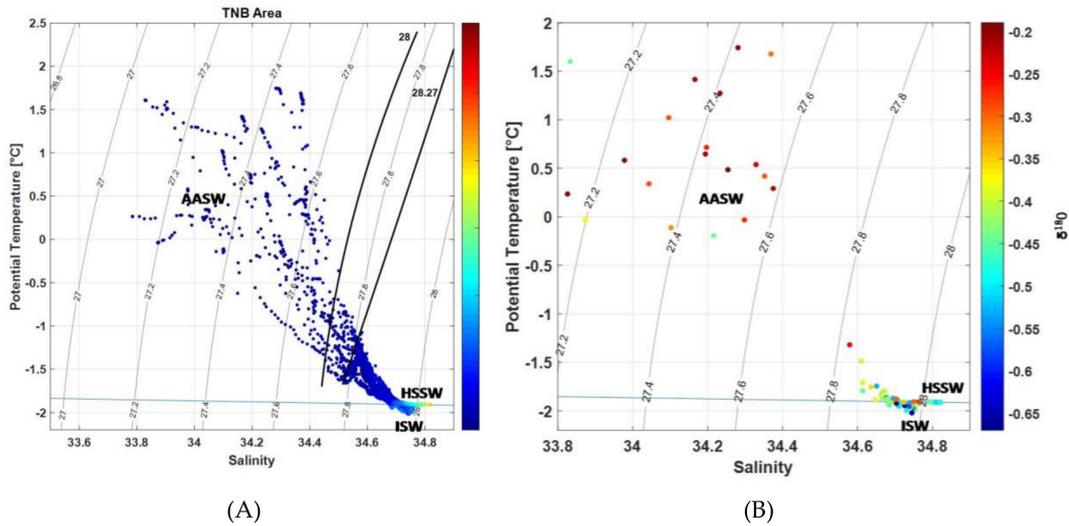

(A)   (B)

Figure 2. θ/S plot of the Terra Nova Bay (TNB) area casts, color-coded by depth (**A**) and δ18O (**B**). Antarctic Surface Water (AASW; γn < 28.00 kg m^{-3} and S < 34.30); High Salinity Shelf Water (HSSW; γn > 28.27 kg m^{-3}, θ < −1.85 °C and S > 34.62); Ice Shelf Water (ISW; θ < −1.93 °C).

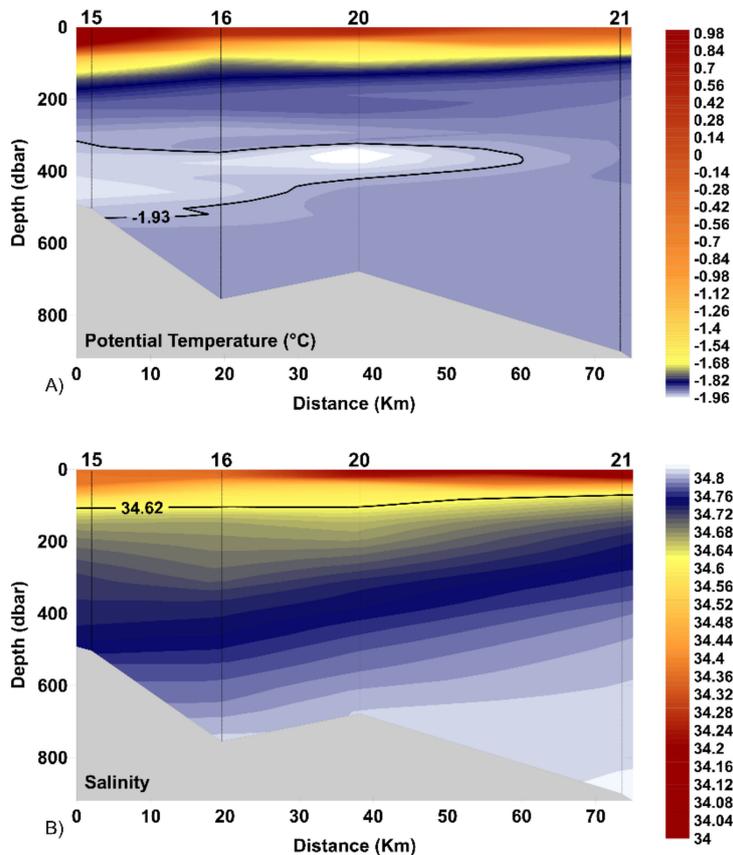**Figure 3.** Distribution of potential temperature (**A**) and salinity (**B**) in 5–21. The −1.93 °C contour line highlights the Terra Nova Bay Ice Shelf Water (TIWS) plume.

3.2. Particulate Trace Metals

Table 2 reports the concentration of SPM and of particulate metals investigated.

Table 2. SPM and particulate metals concentration in the collected samples.

Station	Depth (m)	SPM (mg L^{-1})	Al (nM)	Ba (nM)	Cd (nM)	Cu (nM)	Fe (nM)	Mn (nM)	Ni (nM)	Ti (nM)	Zn (nM)
2	30	0.090	7.07	0.61	0.02	0.36	2.11	0.05	0.07	1.25	0.76
2	100	0.14	11.4	0.33	0.01	0.27	4.36	0.15	0.18	2.55	1.04
2	225	4.53	9.71	0.20	0.07	0.45	11.1	0.34	0.23	5.74	2.09
2	300	1.18	10.6	0.52	0.01	0.15	3.96	0.25	0.24	0.38	1.14
3	20	0.15	5.48	0.42	0.05	0.20	2.13	0.06	0.14	0.38	0.79
3	100	0.13	8.60	0.36	0.02	0.21	2.58	0.11	0.29	0.38	1.57
3	200	4.01	15.5	0.87	0.12	0.43	75.4	0.91	0.59	0.38	1.98
3	350	0.47	8.04	0.31	0.02	0.17	1.90	0.11	0.07	0.38	0.66
6	20	0.96	5.83	0.09	0.03	0.49	1.25	0.04	0.07	0.37	0.54
6	100	0.13	5.99	0.09	0.01	0.04	0.51	0.04	0.07	0.37	0.10
6	240	1.80	9.45	0.16	0.16	0.23	21.0	0.20	0.42	2.04	0.97
6	320	0.52	10.9	0.62	0.08	0.15	3.17	0.04	0.19	0.95	1.25
6	440	0.01	34.2	0.42	0.01	0.07	11.9	0.23	0.07	0.37	0.28
7	20	1.09	9.38	0.22	0.12	0.21	2.69	0.04	0.41	0.37	2.11
7	100	0.25	2.87	0.44	0.01	0.14	2.99	0.09	0.07	0.37	0.38
7	442	0.05	8.65	0.51	0.01	0.04	4.35	0.16	0.07	3.97	0.39
8	212	0.09	4.39	0.15	0.02	0.08	1.29	0.03	0.07	3.38	0.21
8	482	0.04	6.06	0.09	0.02	0.19	2.62	0.11	0.23	2.05	0.10
9	10	1.56	4.47	0.19	0.16	0.24	2.16	0.25	0.41	0.78	2.45
9	220	1.48	2.34	0.09	0.02	0.09	1.55	0.10	0.07	0.38	0.23
9	513	0.09	16.9	0.44	0.01	0.12	7.71	0.38	0.19	1.53	0.22
10	169	0.14	8.51	0.16	0.02	0.19	4.51	0.21	0.20	1.07	0.30
10	242	0.12	7.19	0.17	0.02	0.15	3.75	0.24	0.23	0.38	0.84
10	500	0.09	15.8	0.33	0.01	0.17	6.02	0.65	0.19	1.64	0.33
11	200	0.56	8.22	0.18	0.02	0.27	4.51	0.46	0.07	1.27	0.28
11	240	0.10	11.4	0.23	0.01	0.18	5.28	0.44	0.16	1.15	0.27
11	389	0.14	20.4	0.51	0.02	0.23	6.09	0.46	0.13	9.86	0.38
12	35	0.96	7.34	0.30	0.17	0.35	2.10	0.27	0.34	24.6	1.86
12	280	0.29	4.30	0.09	0.09	0.30	12.0	0.29	0.34	0.38	1.13
12	394	1.79	14.0	0.24	0.04	0.08	5.88	0.19	0.07	6.90	0.57
14	20	1.75	-	4.95	0.02	0.60	-	7.55	0.57	66.2	2.19
14	205	0.06	13.7	0.19	0.01	0.06	6.03	0.12	0.12	0.37	0.10
14	320	1.08	4.32	0.28	0.04	0.11	0.51	0.12	0.19	0.37	0.90
15	40	0.71	7.72	0.09	0.07	0.09	0.51	0.04	0.31	0.37	0.56
15	200	0.29	178	0.79	0.02	0.09	56.2	0.77	0.07	8.28	0.65
15	390	0.13	28.1	0.26	0.01	0.04	10.6	0.20	0.07	1.52	0.10
16	20	0.92	9.73	0.09	0.14	0.14	1.40	0.04	0.33	0.37	1.18
16	300	0.18	88.2	0.41	0.02	0.10	33.3	0.51	0.07	3.55	0.22
16	379	0.06	12.4	0.31	0.01	0.04	5.56	0.19	0.07	0.37	0.23
17	20	0.99	7.16	0.28	0.13	0.32	2.32	0.22	0.41	0.38	1.55
17	240	0.10	57.0	0.29	0.01	0.04	20.1	0.31	0.07	1.92	0.10
17	300	0.05	10.5	0.09	0.01	0.04	0.51	0.04	0.07	0.37	0.10
19	20	1.15	6.16	0.18	0.14	0.32	2.63	0.22	0.39	0.82	1.36
19	191	0.40	31.6	0.33	0.02	0.04	10.4	0.22	0.22	0.37	0.45
19	400	0.14	17.3	0.36	0.01	0.11	5.28	0.33	0.11	2.60	0.28
20	20	1.35	6.30	0.27	0.19	0.35	1.41	0.28	0.60	0.38	1.70
20	288	0.42	14.4	0.23	0.07	0.24	7.42	1.01	0.28	0.91	1.08
20	330	0.02	21.3	0.16	0.02	0.04	6.83	0.18	0.07	0.37	0.10
21	30	1.11	15.2	0.69	0.18	0.42	8.70	0.29	0.47	1.08	3.27
21	300	0.09	33.7	0.57	0.02	0.14	11.1	0.65	0.18	3.05	0.22
22	15	1.32	11.3	0.22	0.14	0.38	4.46	0.33	0.46	0.38	1.58
23	15	1.97	4.82	0.09	0.13	0.37	2.32	3.57	0.43	0.38	3.35
23	252	0.09	10.2	0.28	0.01	0.11	3.05	0.25	0.07	0.38	0.25

Concentration of SPM varied between 0.01 mg L^{-1} (station 20–330 m) and 4.53 mg L^{-1} (station 2–225 m). Generally, the highest concentrations were found in the upper layer of the AASW, except for the sample collected at station 2 at depth of 225 m. The horizontal distribution of SPM in AASW does not follow a clear trend from coast to open sea; however, the lowest concentrations were measured at stations 2 and 3, sampled at the DIT margin. Concentration of pFe ranged between 0.51 nM and 75.44 nM with a minimum value measured at station 6 at 100 m depth and a maximum value at station 3 at 200 m depth. Concentrations of pAl ranged from 2.34 nM and 178.17 nM with a minimum value obtained at station 9 at 220 m depth and a maximum measured at station 15 at 200 m depth. pCu concentrations varied between 0.04 nM and 0.60 nM with a minimum value obtained at station 7 at 442 m depth and a maximum value found close to the surface (20 m depth) at station 14. pMn concentrations varied between 0.03 nM and 7.55 nM with a minimum value obtained at station 7 at a depth of 442 m and a relatively shallow (20 m) maximum value at station 14. pZn concentrations varied between 0.10 nM at station 8 at 482 m depth and 3.35 nM at station 23 at 15 m depth. Figure 4 shows the vertical distribution of SPM and particulate metals for stations 2, 6, 12, 17 and 20, representatives of both more coastal and open sea conditions. There was no common trend in the distribution of SPM and metals. Two principal components were identified by PCA: PC1 explained 47.1% of the total variance, while PC2 explained a further 18.3%. The loadings of the variables on these components (Figure 5A) showed that temperature, fluorescence, dissolved oxygen and $^{\delta 18}$O were negatively correlated with salinity and depth, highlighting that these properties of the AAWS differ significantly from those of deeper water masses. Therefore, samples collected in the AASW were grouped separately from those collected in the HSSW and in TISW (score plot, Figure 5B,C). Particulate trace metals were divided into two groups. The first group had a strong positive load on PC2 and included pAl, pBa, pFe, pMn and pTi (i.e., typical of terrigenous elements), whereas the second group had a negative loading on PC1 and a positive loading on PC2. This group comprises elements of anthropic or biologic origin, such as pCd, pCu, pNi and pZn, along with SPM. In the AASW, a subgroup of samples (stations 12, 21, 22 and 23) was characterized by higher SPM, pCd, pCu, pNi and pZn concentrations compared with other AASW samples. A group of samples collected in deep waters was characterized by high concentrations of pFe, pAl, pBa, pTi and pMn (stations 2, 3, 6, 15 and 20), whereas another group was characterized by high salinity and both low temperature and δ^{18}O values (stations 16, 17, 19 and 20).
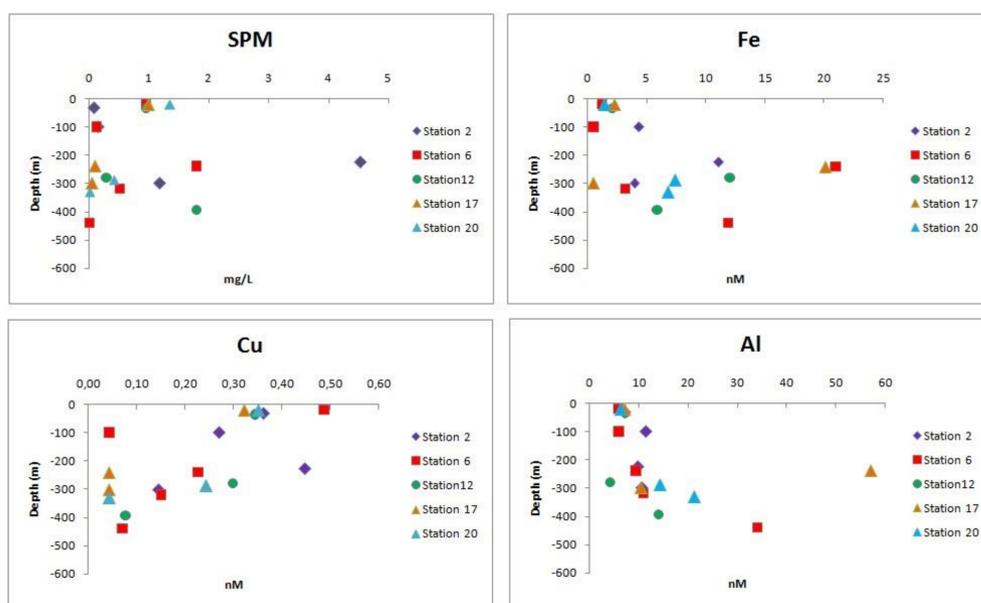

Figure 4. Vertical profiles of SPM (mg L^{-1}) and of pFe, pCu and pAl (nM). Stations 2, 6, 12, 17 and 20 were chosen as representatives.
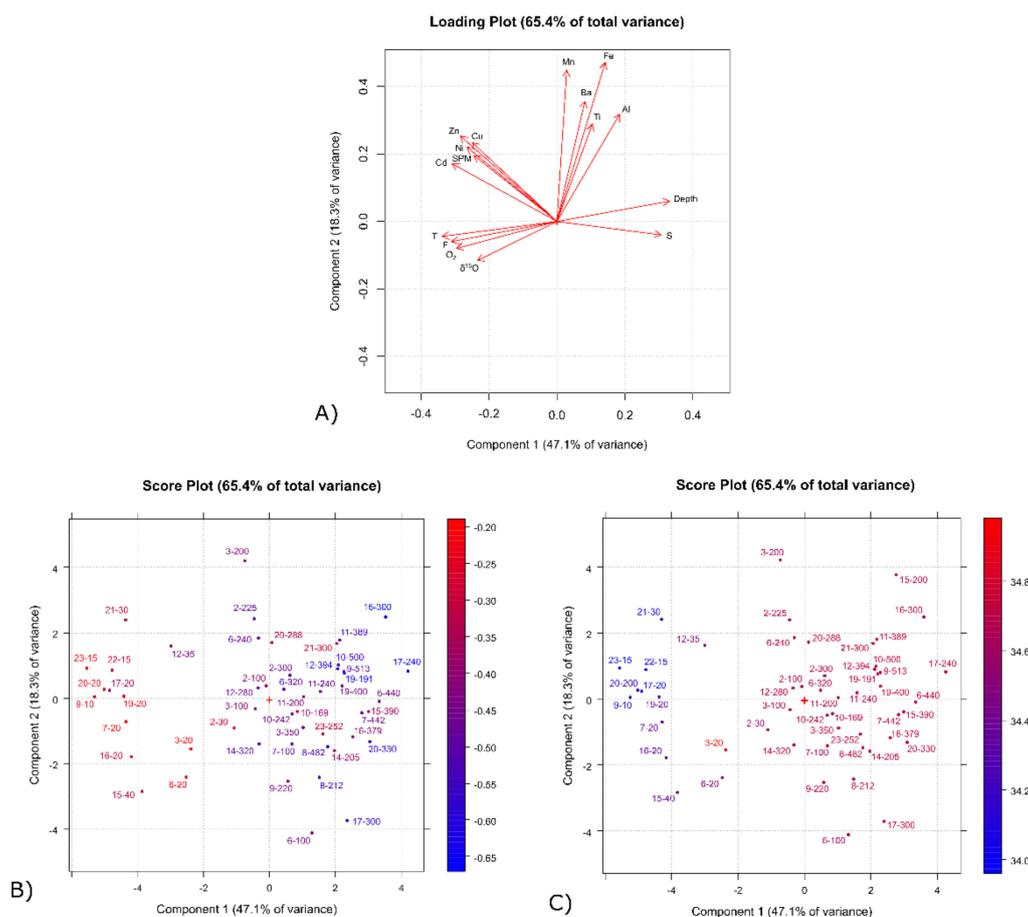
Figure 5. Principal Component Analysis (PCA) plots. (**A**) loading plot; (**B**) score plot, color-coded by δ^{18}O; (**C**) score plot, color-coded by salinity.

Correlations found between SPM, trace metals and environmental parameters were assessed, as summarized in Table 3: pFe correlated positively with depth, salinity, pBa ($p < 0.01$), pAl, pMn and pTi ($p < 0.001$) and negatively with temperature ($p < 0.001$), fluorescence ($p < 0.01$) and with δ^{18}O and O$_2$ ($p < 0.05$). No significant correlation was found between pFe and SPM, pCd, pCu and pZn. SPM was positively correlated with temperature ($p < 0.01$), δ^{18}O ($p < 0.05$), pCu, pCd, pNi and pZn ($p < 0.001$) and negatively correlated with depth, salinity ($p < 0.01$) and pAl ($p < 0.05$). No significant correlation was found with O$_2$, fluorescence and pTi, besides that already mentioned with pFe.

Table 3. Significant correlations (Spearman's) among the variables. Underlined numbers: $p < 0.05$; normal numbers: $p < 0.01$; bold numbers: $p < 0.001$. Grey cells mean no significant correlation.

	Depth	S	T	F	δ^{18}O	O$_2$	SPM	Al	Ba	Cd	Cu	Fe	Mn	Ni	Ti
S	**0.848**														
T	**−0.782**	**−0.729**													
F	**−0.751**	**−0.632**	**0.666**												
δ^{18}O	**−0.658**	**−0.538**	**0.704**	**0.628**											
O$_2$	**−0.555**	−0.384	0.379	**0.588**	0.448										
SPM	−0.517	**−0.603**	0.468	0.213	0.286	0.216									
Al	0.455	0.448	**−0.468**	−0.355	−0.317	−0.154	−0.295								
Ba	0.234	0.264	−0.067	−0.226	−0.098	−0.184	−0.109	**0.49**							
Cd	**−0.583**	**−0.59**	**0.527**	0.447	0.401	0.443	**0.739**	−0.335	−0.194						
Cu	**−0.530**	**−0.543**	**0.572**	0.360	0.466	0.147	**0.572**	−0.333	0.014	**0.648**					
Fe	0.398	0.36	**−0.506**	−0.439	−0.326	−0.336	−0.099	**0.742**	0.409	−0.156	−0.07				
Mn	0.149	0.124	−0.144	−0.177	−0.074	−0.176	0.159	**0.468**	0.315	0.064	0.29	**0.652**			
Ni	−0.464	**−0.502**	**0.533**	0.337	0.373	0.312	**0.579**	−0.182	−0.085	**0.727**	**0.641**	−0.012	0.258		
Ti	0.288	0.245	−0.161	−0.249	−0.284	−0.271	−0.002	0.277	0.317	−0.004	0.158	0.384	0.447	−0.067	
Zn	**−0.565**	**−0.602**	**0.644**	0.385	0.443	0.268	**0.748**	−0.283	0.132	**0.760**	**0.739**	−0.120	0.158	**0.762**	−0.023

4. Discussion

4.1. Particulate Iron in the ASSW

The Ross Sea is made up of a complex mosaic of sub-systems, with physical, chemical, and biological features that change on different temporal and spatial scales [30]. The TNB polynya is a neighboring coastal system, naturally iron fertilized, and supports high primary productivity with implications for regional and basin scale Ross Sea biogeochemistry [21,22,30].

Evidence from recent papers suggests that labile phases of pFe can contribute to the bioavailable Fe pool in the upper water column of different sub systems of the Ross Sea [5,6]. However, an area as particular as TNB (i.e., a coastal polynya located near glaciers) was not considered. Therefore, the data reported herewith contribute not only to understanding iron biogeochemistry in TNB polynya but add information in a more general context.

The distribution of SPM combined with trace metal analysis can give useful information on the mechanisms that supply pFe to coastal water. In surface waters, SPM concentrations were higher and more variable than they were in deep waters. This results largely from the combined effects of an input of externally produced particulates and the internal generation of particulates from primary production, both of which have their strongest signals in coastal waters. pFe concentrations of 0.51–8.70 nM (mean value, 2.58 ± 2.98 nM) were higher than dFe (1.16 ± 0.97) [34] and in agreement with previous data from the Ross Sea [7,12,35,36] and with the shelf-wide mean of 2.9 ± 2.6 nM, reported by Marsay et al., (2017) [6]. Neither SPM nor pFe concentrations showed a coast-open sea trend, confirming the substantial spatial heterogeneity found in previous studies at a horizontal scale of about 10 km, emphasizing the importance of mesoscale physical events to regional biogeochemistry [14,37]. Possible sources of pFe to the TNB AASW include atmospheric continental dust inputs, recently melted sea ice and lateral mixing with water coming from the coast where glacial processes may provide mineral particles. One of the advantages of using the $\delta^{18}O$ isotope method at high latitudes is related to the high depletion of glacial meltwater relative to sea water. Thus, $\delta^{18}O$ is a useful variable to trace glacial melting and related mixing with sea water on the continental shelf [38].The small isotope difference between sea-ice and the surface water that receives melted ice was previously used to distinguish sea-ice melt from meteoric freshwater input, which is isotopically lighter [39].The combination of salinity and calculated MW% with $\delta^{18}O$ data allowed us to establish that the contribution of meteoric freshwater to the decrease in salinity was relevant at stations 8, 10 and 17 only, where a higher lighter isotopic ratio (−0.37–0.44‰) than in other stations (−0.19–0.23 ‰) was measured. Thus, on the basis of $\delta^{18}O$ data and the calculated MW%, we can conclude that sea ice melting was relevant in almost all stations with the exception of the above-mentioned stations and of three coastal stations (6, 15 and 16), where no meltwater addition was obtained by our calculation. The outer stations and station 12 belonged to the AASW sub samples group evidenced by PCA with high SPM and pCd, pCu, pNi and pZn concentrations. Sea ice is fundamental in the biogeochemical cycle of Fe as it accumulates and stores Fe during winter months and releases Fe to surface waters after its' melting. This holds high importance for the biotic component and for the triggering of primary production [11,40]. To evaluate the lithogenic contribution from sea ice, we compared the pFe/pAl ratio in the samples to the reported crustal value. Distinct enrichment of pFe over pAl, as indicated by raised pFe/pAl ratios (0.26–0.58, Figure 6A), was observed in subsurface waters at all stations except the three coastal stations 6, 15 and 16, where no meltwater addition was evidenced and where pFe/pAl values were close to the average Upper Continental Crust (UCC) Fe/Al ratio of 0.19–0.20 [41,42]. This suggests that in these stations dust may have been blown from the land by katabatic winds. On the contrary, in almost all the other stations the pFe cannot be solely of lithogenic origin. Our pFe/pAl ratios fall within the ranges shown for SPM samples collected in the AASW, both from the Ross Sea (0.16–2.36) [7] and the Weddell Sea (0.19–3.2) [42]. Higher values of the lithogenic ratio may indicate the presence of biological material, since the organisms have the ability to bio-concentrate Fe as compared to Al, or they may reflect external inputs of particulate material, for example, of atmospheric origin, in which

the pFe/pAl varies between 0.35 and 0.88 [43]. If it is assumed that all pAl derives from lithogenic material, it is possible to calculate the biogenic iron fraction, which is defined as the difference between total concentration and lithogenic concentration [43]. The biogenic component ranged from 11% at station 20% to 65% at station 23 (Figure 6B), with values ranging from 40% to 60% in the remaining stations. From the comparison with the distribution of fluorescence (Figure 6C), it can be observed that some of the stations with high pFe/pAl values (14–22–23) were characterized by high fluorescence signals too. This indicates the biogenic nature of pFe, as suggested by the positive and significant correlation (Spearman's $p = 0.73$, $p < 0.001$) between fluorescence and chlorophyll-a values reported by Bolinesi et al., (2020) [34]. Further support for the biogenic nature of the SPM is provided by the positive correlation of SPM and fluorescence with pCu (Figure 6D) and pZn (Table 3), which are well-known trace elements with nutrient-type behavior and are actively bio-accumulated in cells [44]. Thus, this biogenic pFe in AASW can contribute significantly to the bioavailable iron pool in TNB because it can be rapidly recycled by microzooplankton, mesozooplankton, viruses and heterotrophic bacteria [45–47]. Moreover, biogenic sinking particles can transfer pFe deeper than the upper mixed layer, where re-mineralization and dissolution can release dFe into the water column.
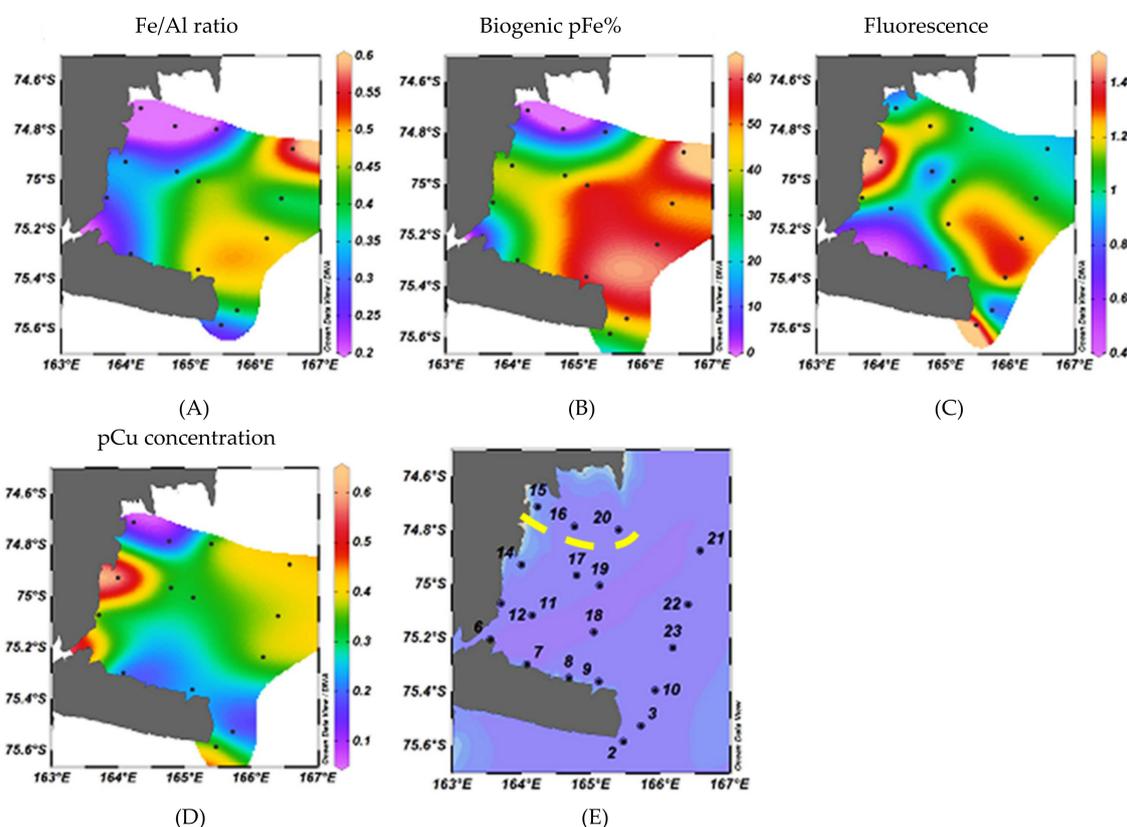
Figure 6. Horizontal distribution of pFe/pAl ratio (**A**), biogenic pFe (%) (**B**), fluorescence (**C**), and pCu concentration (nM) (**D**). Stations without a melting addition have been yellow framed in panel (**E**).

4.2. Particulate Iron in the Shelf Waters

Analysis of SPM collected in shelf waters showed pFe concentrations of 0.51–75.4 nM (mean value 9.54 ± 13.6 nM)—always higher than AASW. Strong correlations among lithogenic elements in SPM (Table 3) and strong apportionment in PCA (Figure 4, panel A) suggested an important role for lithogenic particles in controlling metal distributions in selected stations, besides the sinking of biogenic particles. Thus, melting of proximal glaciers in TNB has been considered in this study as a potential source of pFe for the water column. In fact, the melting at the base of the continental glacier and/or the melting of the ice shelf underside could release Fe from a sediment-rich layer of basal

ice, both processes potentially contributing to the increase of pFe and dFe in the sub-euphotic zone. In particular, this can occur through the release of accumulated atmospheric dust and material eroded from the bottom of the glacier [10,48]. pFe in TISW averaged 11.7 ± 9.2 nM, resulting in a relatively higher concentration than pFe in HSSW (5.55 ± 4.43 nM). Moreover, our data from TISW samples were higher than those reported by Marsay et al., (2017) [6] for Ice Shelf Waters (ISW) samples collected along the Ross Ice Shelf (2.7 ± 1.5 nM), suggesting that the drainage of material released from the Reeves, Priestley and David Glaciers could be relevant in terms of pFe contribution to the deep layer in the TNB area. Information on the origin of pFe can be obtained by comparing the pFe/pAl ratio in the samples to the reported crustal value, even in the case of deep waters, together with the pMn/pAl ratio used for estimating the presence of oxides. The pFe/pAl ratio was higher than the average UCC Fe/Al ratio for both TISW and HSSW samples, also showing high variability (0.12–2.80 and 0.05–2.22 for TISW and HSSW, respectively), suggesting that much of the pFe was not lithogenic material. We calculated the contribution of lithogenic Fe to pFe, which accounted for ~49 ± 17% in both water masses. Similarly, the average pMn/pAl ratio was 0.011 (average crustal value 0.0034), suggesting an increase in Mn due to the formation of authigenic phases in the water column. The pMn/pAl ratio is comparable to the values obtained for SPM samples collected in the Amundsen Sea in correspondence to ISW outflow (0.006–0.221), in which microscopic and mineralogical analyses had highlighted the presence of crustal particles deriving from the erosion of the glacier on the seabed, which was enriched with oxides and hydroxides [42]. Raised pFe/pAl ratios with respect to crustal value may indicate both a hydroxides and iron oxides contribution and a biogenic contribution due to the settlement of organisms from the euphotic layer. The biogenic contribution to the particulate was confirmed, for instance, at station 12 by FE-SEM analysis, showing the presence of diatom frustules (Figure 7A). The data is in agreement with the results on particulate matter collected in sediment traps in the Ross Sea at depths of between 200 and 540 m, mainly consisting of biogenic silica [49]. However, FE-SEM analysis showed the presence of nanoparticle aggregates, which also sustains the hypothesis of a lithogenic contribution to the particulate matter (Figure 7B,C). Although the analyzed spots are probably nanoparticle aggregates, the presence of zirconium in some nanoparticles on diatom frustules (spots 15 and 16 in Figure 7A) is probably related to Zr-rich minerals such as Baddeleyite (ZrO_2) along with (spot 15) Cr-Ni-bearing particles.

The lithogenic fraction reached the 59% of the pFe at station 20 (pFe/pAl 0.32), where the FE-SEM analysis (spots 1 and 2 in Figure 8A) revealed the presence of Fe-rich Cr- Ni- bearing particles, likely spinels (Figure 8B,C).

Spinels group represents oxide minerals with generic formula AB_2O_4, where A represents bivalent cations (e.g., Fe, Mg, Mn, Ni, Ti and Zn) and B trivalent cations (e.g., Al, Cr, Fe and Mn) (see [50] for a detailed spinel-type minerals overview). Cr- and Ni-bearing spinels are common accessory minerals in mafic and ultramafic rocks. In the literature, there are few studies concerning the morphology and crystalline structure of particulate matter present in glacial sediments [51], in which a high variability in the type and size of the SPM was observed. In most cases, iron-rich phases are present in the aggregates of nanoparticles between 50 and 250 nm in diameter. Glacial sediments can contain different minerals rich in Fe(II). Particles containing oxides, olivine and spinels rich in Fe(II) were found in our samples. The mineralogical composition of the particulate material released by glacial melting is like the soil on which the glacier has slipped and carried out an erosive process. The minerals identified in the soils surrounding TNB were plagioclase, alkaline feldspars, pyroxene and olivine. Furthermore, the presence of basaltic rocks particularly rich in Fe, Mg, Cr and Ni was also found [52]. Therefore, the minerals identified in our samples have the mineralogical composition of surrounding soils, suggesting that lithogenic material scoured by glaciers can contribute to the amount of iron in the deep-water column. The speciation and mineralogy of pFe is particularly important for determining its bioavailability; recent studies suggest that the particulate Fe(II) pool may play a significant role in the iron biogeochemical cycle. The most potentially bioavailable Fe is delivered as poorly ordered oxyhydroxide nanoparticles, primarily ferrihydrite that has already been demonstrated to be, at least to

some degree, bioavailable to phytoplankton cultures [53]. Thus, the Fe(II) contained in mineral particles is potentially environmentally available due to the instability of Fe(II) in the oxidizing conditions of Antarctic waters.
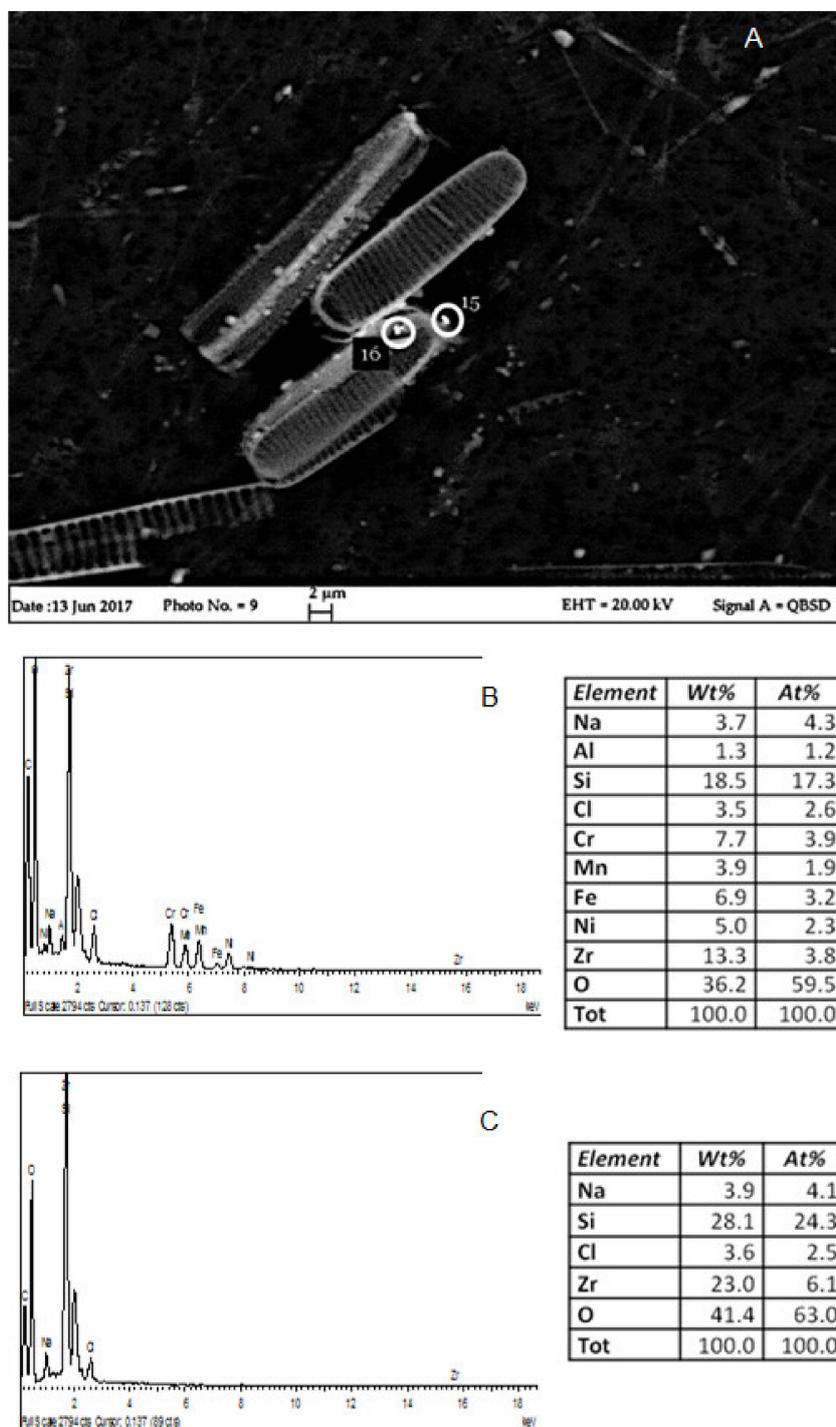

A

Date :13 Jun 2017   Photo No. = 9   2 µm   EHT = 20.00 kV   Signal A = QBSD

B

Element	Wt%	At%
Na	3.7	4.3
Al	1.3	1.2
Si	18.5	17.3
Cl	3.5	2.6
Cr	7.7	3.9
Mn	3.9	1.9
Fe	6.9	3.2
Ni	5.0	2.3
Zr	13.3	3.8
O	36.2	59.5
Tot	100.0	100.0

C

Element	Wt%	At%
Na	3.9	4.1
Si	28.1	24.3
Cl	3.6	2.5
Zr	23.0	6.1
O	41.4	63.0
Tot	100.0	100.0

Figure 7. FE-SEM image and Energy Dispersive Spectroscopy (EDS) spectra of selected points of sample station 12–394 m. (**A**) Large scale FE-SEM image of sample; (**B**) EDS spectrum and elemental composition of point 15; (**C**) EDS spectrum and elemental composition of point 16 (*Wt%* = weight percentage; *At%* = atomic percentage).

Element	Wt%	At%
Cr	12.2	8.2
Mn	1.9	1.2
Fe	54.4	34.0
Ni	7.6	4.5
O	23.9	52.1
Tot	100.0	100.0

Element	Wt%	At%
Cr	12.7	8.5
Fe	56.2	35.1
Ni	7.2	4.3
O	23.9	52.1
Tot	100.0	100.0
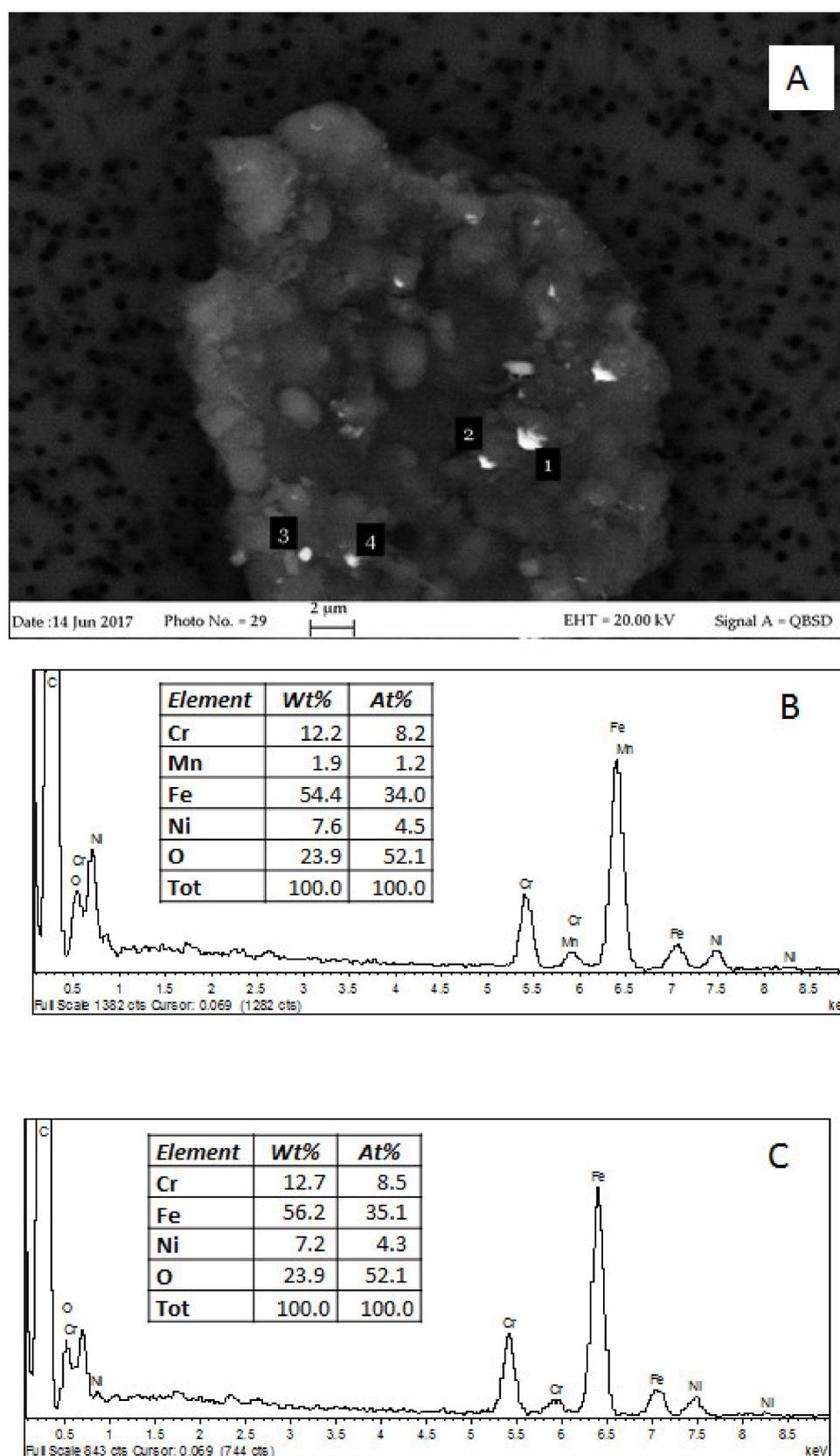
Figure 8. FE-SEM image and EDS spectra of selected points of sample station 20–330 m. (**A**) Large-scale FE-SEM image of sample; (**B**) EDS spectrum and elemental composition of point 1; (**C**) EDS spectrum and elemental composition of point 2 (*Wt%* = weight percentage; *At%* = atomic percentage).

5. Conclusions

This study provides insight into the biogeochemistry of the Terra Nova Bay area, highlighting the spatial heterogeneity of both SPM and particulate metals concentration in the water masses. The meltwater in surface waters can contribute to the particulate iron pool both in terms of lithogenic combined with dust blown from the land by katabatic winds and biogenic forms. This biogenic iron could contribute significantly to the bioavailable iron pool sustaining primary production in this area. Moreover, biogenic sinking particles can transfer pFe deeper than the upper mixed layer, where re-mineralization and dissolution can release dFe into the water column. TISW is characterized by a concentration of pFe that is higher than both HSSW and Ross Ice Shelf ISW. The lithogenic material associated with TISW represents an additional source of pFe for the deep layer of the Terra Nova Bay water column. This suggests that the drainage of material released from the Reeves, Priestley and David Glaciers could be relevant in terms of pFe contribution. Future expected increasing melt rates of these glaciers may increase Fe input, thus playing a greater role in supplying iron and counteracting the reductions in sea ice cover around Terra Nova Bay. Important questions still to be addressed are the fate meltwater particulate iron introduced into the coastal polar ocean, how bioavailable the particulate forms of introduced Fe are, and the factors controlling the interplay between particulate and dissolved iron in the upper waters.

References

1. Parekh, P.; Follows, M.J.; Boyle, E.A. Decoupling of iron and phosphate in the global ocean. *Glob. Biogeochem. Cycles* **2005**, *19*. [CrossRef]

2. Gerringa, L.; Rijkenberg, M.; Schoemann, V.; Laan, P.; De Baar, H. Organic complexation of iron in the West Atlantic Ocean. *Mar. Chem.* **2015**, *177*, 434–446. [CrossRef]

3. McGillicuddy, D.J.J.; Sedwick, P.N.; Dinniman, M.S.; Arrigo, K.R.; Bibby, T.S.; Greenan, B.J.W.; E Hofmann, E.; Klinck, J.M.; O Smith, W.; Mack, S.L.; et al. Iron supply and demand in an Antarctic shelf ecosystem. *Geophys. Res. Lett.* **2015**, *42*, 8088–8097. [CrossRef]

4. De Jong, J.; Schoemann, V.; Maricq, N.; Mattielli, N.; Langhorne, P.; Haskell, T.; Tison, J.-L. Iron in land-fast sea ice of McMurdo Sound derived from sediment resuspension and wind-blown dust attributes to primary productivity in the Ross Sea, Antarctica. *Mar. Chem.* **2013**, *157*, 24–40. [CrossRef]

5. Noble, A.E.; Moran, D.M.; Allen, A.E.; Saito, M.A. Dissolved and particulate trace metal micronutrients under the McMurdo Sound seasonal sea ice: Basal sea ice communities as a capacitor for iron. *Front. Chem.* **2012**, *1*, 25. [CrossRef]

6. Marsay, C.M.; Barrett, P.M.; McGillicuddy, D.J.J.; Sedwick, P.N. Distributions, sources, and transformations of dissolved and particulate iron on the Ross Sea continental shelf during summer. *J. Geophys. Res. Oceans* **2017**, *122*, 6371–6393. [CrossRef]

7. Fitzwater, S.; Johnson, K.; Gordon, R.; Coale, K.; Smith, W. Trace metal concentrations in the Ross Sea and their relationship with nutrients and phytoplankton growth. *Deep. Sea Res. Part II: Top. Stud. Oceanogr.* **2000**, *47*, 3159–3179. [CrossRef]

8. Atkins, C.B.; Dunbar, G.B. Aeolian sediment fl ux from sea ice into Southern McMurdo Sound, Antarctica. *Glob. Planet. Chang.* **2009**, *69*, 133–141. [CrossRef]

9. Smith, W.; Sedwick, P.; Arrigo, K.; Ainley, D.; Orsi, A. The Ross Sea in a Sea of Change. *Oceanography* **2012**, *25*, 90–103. [CrossRef]

10. Rignot, E.; Jacobs, S.; Mouginot, J.; Scheuchl, B. Ice-Shelf Melting Around Antarctica. *Science* **2013**, *341*, 266–270. [CrossRef]

11. Grotti, M.; Soggia, F.; Ianni, C.; Frache, R. Trace metals distributions in coastal sea ice of Terra Nova Bay, Ross Sea, Antarctica. *Antarct. Sci.* **2005**, *17*, 289–300. [CrossRef]

12. Rivaro, P.; Ianni, C.; Massolo, S.; Abelmoschi, M.L.; De Vittor, C.; Frache, R. Distribution of dissolved labile and particulate iron and copper in Terra Nova Bay polynya (Ross Sea, Antarctica) surface waters in relation to nutrients and phytoplankton growth. *Cont. Shelf Res.* **2011**, *31*, 879–889. [CrossRef]

13. Rivaro, P.; Abelmoschi, M.L.; Grotti, M.; Ianni, C.; Magi, E.; Margiotta, F.; Massolo, S.; Saggiomo, V. Combined effects of hydrographic structure and iron and copper availability on the phytoplankton growth in Terra Nova Bay Polynya (Ross Sea, Antarctica). *Deep. Sea Res. Part I: Oceanogr. Res. Pap.* **2012**, *62*, 97–110. [CrossRef]

14. Rivaro, P.; Ardini, F.; Grotti, M.; Aulicino, G.; Cotroneo, Y.; Fusco, G.; Mangoni, O.; Bolinesi, F.; Saggiomo, M.; Celussi, M. Mesoscale variability related to iron speciation in a coastal Ross Sea area (Antarctica) during summer 2014. *Chem. Ecol.* **2019**, *35*, 1–19. [CrossRef]

15. Budillon, G.; Gremes Cordero, S.; Salusti, E. On The Dense Water Spreading Off The Ross Sea Shelf (Antarctica). *J. Mar. Syst.* **2002**, *35*, 207–227. [CrossRef]

16. Petrelli, P.; Bindoff, N.L.; Bergamasco, A. The sea ice dynamics of Terra Nova Bay and Ross Ice Shelf Polynyas during a spring and winter simulation. *J. Geophys. Res. Space Phys.* **2008**, *113*, 1–16. [CrossRef]

17. Frezzotti, M.; Mabin, M.C.G. 20th century behaviour of Drygalski Ice Tongue, Ross Sea, Antarctica. *Ann. Glaciol.* **1994**, *20*, 397–400. [CrossRef]

18. Sansiviero, M.; Maqueda, M.M.; Fusco, G.; Aulicino, G.; Flocco, D.; Budillon, G. Modelling sea ice formation in the Terra Nova Bay polynya. *J. Mar. Syst.* **2017**, *166*, 4–25. [CrossRef]

19. Misic, C.; Harriague, A.C.; Mangoni, O.; Aulicino, G.; Castagno, P.; Cotroneo, Y. Effects of physical constraints on the lability of POM during summer in the Ross Sea. *J. Mar. Syst.* **2017**, *166*, 132–143. [CrossRef]

20. Budillon, G.; Castagno, P.; Aliani, S.; Spezie, G.; Padman, L. Thermohaline variability and Antarctic bottom water formation at the Ross Sea shelf break. *Deep. Sea Res. Part I Oceanogr. Res. Pap.* **2011**, *58*, 1002–1018. [CrossRef]

21. Castagno, P.; Capozzi, V.; DiTullio, G.R.; Falco, P.; Fusco, G.; Rintoul, S.R.; Spezie, G.; Budillon, G. Rebound of shelf water salinity in the Ross Sea. *Nat. Commun.* **2019**, *10*, 1–6. [CrossRef] [PubMed]

22. Silvano, A.; Foppert, A.; Rintoul, S.R.; Holland, P.R.; Tamura, T.; Kimura, N.; Castagno, P.; Falco, P.; Budillon, G.; Haumann, F.A.; et al. Recent recovery of Antarctic Bottom Water formation in the Ross Sea driven by climate anomalies. *Nat. Geosci.* **2020**, *13*, 780–786. [CrossRef]

23. Orsi, A.H.; Wiederwohl, C.L. A recount of Ross Sea waters. *Deep. Sea Res. Part II Top. Stud. Oceanogr.* **2009**, *56*, 778–795. [CrossRef]

24. Budillon, G.; Spezie, G. Thermohaline structure and variability in the Terra Nova Bay polynya, Ross Sea. *Antarct. Sci.* **2000**, *12*, 493–508. [CrossRef]

25. Tremblay, J.-E.; Smith, W. *Primary Production and Nutrient Dynamics in Polynyas*; Elsevier Oceanography Series; Elsevier: Amsterdam, The Netherlands, 2007; Chapter 8; Volume 74, pp. 239–269.

26. Saggiomo, M.; Poulin, M.; Mangoni, O.; Lazzara, L.; De Stefano, M.; Sarno, D.; Zingone, A. Spring-time dynamics of diatom communities in landfast and underlying platelet ice in Terra Nova Bay, Ross Sea, Antarctica. *J. Mar. Syst.* **2017**, *166*, 26–36. [CrossRef]

27. SCOR Working Group. *The Acquisition, Calibration and Analysis of CTD Data*; UNESCO: Paris, France, 1988; p. 102.

28.	Fofonoff, N.P.; Millard, R.C., Jr. *Algorithms for Computation of Fundamental Properties of Seawater*; UNESCO: Paris, France, 1983; Volume 44.

29.	Planquette, H.; Sherrell, R.M. Sampling for particulate trace element determination using water sampling bottles: Methodology and comparison to in situ pumps. Limnol. Oceanogr. *Methods* **2012**, *10*, 367–388.

30.	Grasshoff, K.; Kremling, K.; Ehrhardt, M. *Methods of Seawate Analysis*; Wiley Online Library: Hoboken, NJ, USA, 1983.

31.	Bazzano, A.; Rivaro, P.; Soggia, F.; Ardini, F.; Grotti, M. Anthropogenic and natural sources of particulate trace elements in the coastal marine environment of Kongsfjorden, Svalbard. *Mar. Chem.* **2014**, *163*, 28–35. [CrossRef]

32.	Jackett, D.R.; McDougall, T.J. A Neutral Density Variable for the World's Oceans. *J. Phys. Oceanogr.* **1997**, *27*, 237–263. [CrossRef]

33.	Leardi, R.; Melzi, C.; Polotti, G. Chemometric Agile Tool (CAT). 2017. Available online: http: //gruppochemiometria.it/index.php/software (accessed on 14 November 2020).

34.	Bolinesi, F.; Saggiomo, M.; Ardini, F.; Castagno, P.; Cordone, A.; Fusco, G.; Mangoni, O. Spatial-Related Community Structure and Dynamics in Phytoplankton of The Ross Sea, Antarctica. *Front. Mar. Sci.* **2020**, *7*, 1092.

35.	Ianni, C.; Rivaro, P.; Frache, R. Distribution of Dissolved and Particulate Iron, Copper and Manganese in the Shelf Waters of the Ross Sea (Antarctica). *Mar. Ecol.* **2002**, *23*, 210–219. [CrossRef]

36.	Corami, F.; Capodaglio, G.; Turetta, C.; Soggia, F.; Magi, E.; Grotti, M. Summer distribution of trace metals in the western sector of the Ross Sea, Antarctica. *J. Environ. Monit.* **2005**, *7*, 1256. [CrossRef] [PubMed]

37.	Rivaro, P.; Ianni, C.; Langone, L.; Ori, C.; Aulicino, G.; Cotroneo, Y.; Saggiomo, M.; Mangoni, O. Physical and biological forcing of mesoscale variability in the carbonate system of the Ross Sea (Antarctica) during summer 2014. *J. Mar. Syst.* **2017**, *166*, 144–158. [CrossRef]

38.	Dini, M.; Stenni, B. Oxygen Isotope Characterization of Terra Nova Bay Seawater. In *Ross Sea Ecology*; Springer: Berlin/Heidelberg, Germany, 2000; pp. 27–37.

39.	Meredith, M.P.; Brandon, M.A.; Wallace, M.I.; Clarke, A.; Leng, M.J.; Renfrew, I.A.; King, J.C. Variability in the freshwater balance of northern Marguerite Bay, Antarctic Peninsula: Results from delta-18O. *Deep Sea Res. Part II Top. Stud. Oceanogr.* **2008**, *55*, 309–322. [CrossRef]

40.	Lannuzel, D.; Schoemann, V.; De Jong, J.; Tison, J.-L.; Chou, L. Distribution and biogeochemical behaviour of iron in the East Antarctic sea ice. *Mar. Chem.* **2007**, *106*, 18–32. [CrossRef]

41.	Wedepohl, K.H. The composition of the continental crust. *Geochim. Cosmochim. Acta* **1995**, *59*, 1217–1232. [CrossRef]

42.	Planquette, H.; Sherrell, R.M.; E Stammerjohn, S.; Field, M.P. Particulate iron delivery to the water column of the Amundsen Sea, Antarctica. *Mar. Chem.* **2013**, *153*, 15–30. [CrossRef]

43.	Planquette, H.; Fones, G.R.; Statham, P.J.; Morris, P.J. Origin of iron and aluminium in large particles (>53 μm) in the Crozet region, Southern Ocean. *Mar. Chem.* **2009**, *115*, 31–42. [CrossRef]

44.	Sherrell, R.M.; Lagerstrom, M.; Forsch, K.; E Stammerjohn, S.; Yager, P.L. Dynamics of dissolved iron and other bioactive trace metals (Mn, Ni, Cu, Zn) in the Amundsen Sea Polynya, Antarctica. *Elem. Sci. Anth.* **2015**, *3*, 1–27. [CrossRef]

45.	Umani, S.F.; Monti, M.; Nuccio, C. Microzooplankton biomass distribution in Terra Nova Bay, Ross Sea (Antarctica). *J. Mar. Syst.* **1998**, *17*, 289–303. [CrossRef]

46.	Celussi, M.; Cataletto, B.; Umani, S.F.; Del Negro, P. Deep-Sea Research I Depth profiles of bacterioplankton assemblages and their activities in the Ross Sea. *Deep Sea Res. Part I Oceanogr. Res. Pap.* **2009**, *56*, 2193–2205. [CrossRef]

47.	Boyd, P.W.; Ellwood, M.J. The biogeochemical cycle of iron in the ocean. *Nat. Geosci.* **2010**, *3*, 675–682. [CrossRef]

48.	Sedwick, P.N.; DiTullio, G.R.; Mackey, D.J. Iron and manganese in the Ross Sea, Antarctica: Seasonal iron limitation in Antarctic shelf waters. *J. Geophys. Res. Space Phys.* **2000**, *105*, 11321–11336. [CrossRef]

49.	Langone, L.; Frignani, M.; Ravaioli, M.; Bianchi, C. Particle fluxes and biogeochemical processes in an area influenced by seasonal retreat of the ice margin (northwestern Ross Sea, Antarctica). *J. Mar. Syst.* **2000**, *27*, 221–234. [CrossRef]

50.	Biagioni, C.; Pasero, M. The systematics of the spinel-type minerals: An overview. *Am. Mineral.* **2014**, *99*, 1254–1264. [CrossRef]

51. Monien, D.; Monien, P.; Brünjes, R.; Widmer, T.; Kappenberg, A.; Busso, A.A.S.; Schnetger, B.; Brumsack, H.-J. Meltwater as a source of potentially bioavailable iron to Antarctica waters. *Antarct. Sci.* **2017**, *29*, 277–291. [CrossRef]

52. Malandrino, M.; Abollino, O.; Buoso, S.; Casalino, C.E.; Gasparon, M.; Giacomino, A.; La Gioia, C.; Mentasti, E. Geochemical characterisation of Antarctic soils and lacustrine sediments from Terra Nova Bay. *Microchem. J.* **2009**, *92*, 21–31. [CrossRef]

53. Hawkings, J.; Benning, L.G.; Raiswell, R.; Kaulich, B.; Araki, T.; Kazemian, M.; Stockdale, A.; Koch-Müller, M.; Wadham, J.L.; Tranter, M. Biolabile ferrous iron bearing nanoparticles in glacial sediments. *Earth Planet. Sci. Lett.* **2018**, *493*, 92–101. [CrossRef]